HHS Public Access

Author manuscript

Bioconjug Chem. Author manuscript; available in PMC 2019 April 02.

Published in final edited form as:

Bioconjug Chem. 2018 July 18; 29(7): 2309–2315. doi:10.1021/acs.bioconjchem.8b00292.

Radioligand Therapy of Prostate Cancer with a Long-Lasting Prostate-Specific Membrane Antigen Targeting Agent ^{90}Y-DOTA-EB-MCG

Zhantong Wang[†], **Orit Jacobson**[†], **Rui Tian**[†], **Ronnie C. Mease**[‡], **Dale O. Kiesewetter**[†], **Gang Niu**[*,†], **Martin G. Pomper**[‡], and **Xiaoyuan Chen**[*,†]

[†]Laboratory of Molecular Imaging and Nanomedicine, National Institute of Biomedical Imaging and Bioengineering (NIBIB), National Institutes of Health (NIH), Bethesda, Maryland 20892, United States

[‡]Department of Radiology and Radiological Science, Johns Hopkins Medical Institutions, Baltimore, Maryland 21205, United States

Abstract

Several radioligands targeting prostate-specific membrane antigen (PSMA) have been clinically introduced as a new class of radiotheranostics for the treatment of prostate cancer. Among them, (((*R*)-1-carboxy-2-mcercaptoethyl)carbamoyl)-L-glutamic acid (MCG) has been successfully labeled with radioisotopes for prostate cancer imaging. The aim of this study is to conjugate MCG with an albumin binding moiety to further improve the in vivo pharmacokinetics. MCG was conjugated with an Evans blue (EB) derivative for albumin binding and a DOTA chelator. PSMA positive (PC3-PIP) and PSMA negative (PC3) cells were used for both in vitro and in vivo studies. Longitudinal PET imaging was performed at 1, 4, 24, and 48 h post-injection to evaluate the biodistribution and tumor uptake of ^{86}Y-DOTA-EB-MCG. DOTA-EB-MCG was also labeled with ^{90}Y for radionuclide therapy. Besides tumor growth measurement, tumor response to escalating therapeutic doses were also evaluated by immunohistochemistry and fluorescence microscopy. Based on quantification from ^{86}Y-DOTA-EB-MCG PET images, the tracer uptake in PC3-PIP tumors increased from 22.33 ± 2.39%ID/g at 1 h post-injection (p.i.), to the peak of 40.40 ± 4.79%ID/ g at 24 h p.i. Administration of 7.4 MBq of ^{90}Y-DOTA-EB-MCG resulted in significant regression of tumor growth in PSMA positive xenografts. No apparent toxicity or body weight loss was observed in all treated mice. Modification of MCG with an Evans blue derivative

[*]**Corresponding Authors** niug@mail.nih.gov. [*] shawn.chen@nih.gov.

ASSOCIATED CONTENT

Supporting Information

The Supporting Information is available free of charge on the ACS Publications website at DOI: 10.1021/acs.bioconj-chem.8b00292.

Supporting methods and materials; hematologic analysis of blood samples from untreated and treated mice; flowcytometry of PMSA positive PC3-PIP and PMSA negative PC3 cells; Immunofluorescence staining of tumor sections originated from PC3-PIP and PC3 cells; biodistribution of ^{86}Y-DOTA-MCG and ^{86}Y-EB-DOTA- MCG in normal organs and PSMA positive/negative tumors at 48 h p.i.; changes of body weight of PC3 PIP tumor bearing mice after radioligand treatment; H&E staining of tissue sections from different groups (PDF)

Notes

The authors declare no competing financial interest.

resulted in a highly efficient prostate cancer targeting agent (EB-MCG), which showed great potential in prostate cancer treatment after being labeled with therapeutic radioisotopes.

Graphical Abstract

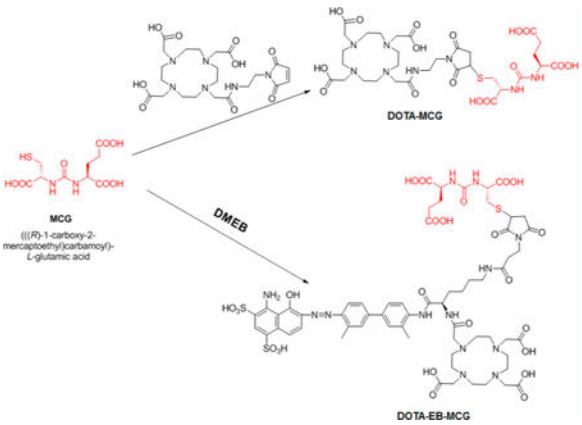

INTRODUCTION

Prostate cancer is the second most frequently diagnosed cancer in men and the fifth leading cause of death worldwide.[1] Although various treatment methods are available for prostate cancer depending on the stage of the disease, such as surgery, prostate brachytherapy, hormonal therapy, chemotherapy, and different combinations of these, relapses occur in approximately 90% of prostate cancer patients after primary therapy.[2] Recently, prostate-specific membrane antigen (PSMA) targeted radionuclide therapy has been demonstrated to be a well-tolerated and effective therapeutic option in patients with metastatic castration-resistant prostate cancer (mCRPC).[3]

PSMA, also known as type II membrane metalloenzyme (glutamate carboxypeptidase II), is significantly overexpressed on the cell membrane of nearly all prostate cancer cells. Moreover, PSMA expression level increases with the stage and grade of the tumor.[4] Therefore, a wide variety of imaging and therapeutic agents ranging from antibodies to low-molecular-weight compounds with PSMA as target have been extensively studied.[5] Low-molecular-weight compounds targeting PSMA are gaining the most popularity due to the comparable binding affinity with PSMA, improved pharmacokinetics, and effective internalization via clathrin coated pits, as compared to the high-molecular-weight counterparts.[6] Several small molecular scaffolds have been developed and can be divided into three categories: thiol-based, phosphorus-based, and urea-based. Among them, urea-based PSMA targeting compounds have higher binding affinity over the other two classes of compounds. Therefore, several urea-based PSMA targeting agents have been clinically introduced for imaging and treating prostate cancer.[7,8]

There have been more than 1000 therapy cycles performed using ^{177}Lu radioligand therapy (RLT) targeting PSMA and the retrospective evidence of dosimetry, safety, and efficacy has been reported.[3,9,10] So far, ^{177}Lu-PSMA-617 and ^{177}Lu-PSMA I&T are the two most commonly used PSMA ligands for clinical RLT and both ligands demonstrated prolonged

accumulation in lesions of prostate cancer. However, high uptake in the kidneys, lacrimal glands, salivary glands, and proximal small bowel are also found with both compounds.[11,12] One strategy to further improve the pharmacokinetics of ^{177}Lu-labeled small molecular PSMA ligands is through conjugation of an albumin binding moiety, with the aim to increase tumor accumulation and retention and decrease nontarget binding of the radiopharmaceutical. For example, a ^{177}Lu-labeled phosphoramidate-based PSMA inhibitor has been conjugated with an albumin-binding motif, 4-(*p*-iodophenyl)butyric acid, to achieve increased circulation half-life and prostate tumor uptake.[13] The same albumin binding motif has also been conjugated to a urea-based PSMA-binding entity, PSMA-617, resulting in higher tumor uptake. However, the kidney accumulation of the newly synthesized compounds was also much higher than that of PSMA-617.[14,15]

We have developed an alternative albumin binding moiety, based on the structure of Evans blue dye.[16–20] One of our truncated Evans blue (tEB) derivative was conjugated to octreotate peptide, and resulted in a significant improvement of its pharmacokinetics, tumor uptake, and therapeutic effect.[21,22]

MCG is a urea-based compound first synthesized by Kozikowski et al. in 2001[23] as an inhibitor of glutamate carboxy peptidase II, which is a very similar enzyme to PSMA. This compound has been labeled with ^{11}C and ^{18}F for PET imaging of PSMA.[24–26] In this study, we conjugated tEB moiety onto MCG, together with a macrocyclic chelator DOTA, with the aim of developing a long-lasting PSMA targeting compound for RLT of prostate cancer (Figure 1). Both the pharmacokinetics and pharmacodynamics of the new compound were investigated in tumor xenografted mice, in comparison with unmodified MCG.

RESULTS

Synthesis of PSMA Ligands.

DOTA-MCG was obtained by conjugating MCG with DOTA-maleimide. The other PSMA ligand with albumin binding motif, truncated Evans blue, was synthesized by conjugating MCG with DOTA-Maleimide-EB (DMEB) previously reported by us.[21]

In Vitro Characterization of PSMA Ligands.

The binding affinities of two ligands DOTA-MCG and DOTA-EB-MCG to PMSA were tested in PSMA-negative PC3 and PSMA-positive PC3-PIP cells, in which the PSMA expression levels were evaluated by flow cytometry. The difference of PSMA expression was also confirmed by immunofluorescence staining on sections from PC3 and PC3-PIP tumors (Figure S1). As shown in Figure 1A, the IC_{50} values for DOTA-MCG and DOTA-EB-MCG were 13.5 and 15.6 nM, respectively. The results indicated that the conjugation of albumin binding motif to MCG did not affect the binding for PSMA.

The uptake and internalization of ^{86}Y-DOTA-MCG and ^{86}Y-DOTA-EB-MCG were tested with PC3-PIP cells. Both ^{86}Y-DOTA-MCG and ^{86}Y-DOTA-EB-MCG showed increasing uptake and internalization along with incubation time to 24 h. ^{86}Y-DOTA-EB-MCG showed much higher uptake value over ^{86}Y-DOTA-MCG at all the time points measured, especially at 24 h (Figure 1B,C). The specificities of ^{86}Y-DOTA-MCG and ^{86}Y-DOTA-EB-MCG

binding with PSMA were confirmed by coincubation with excess amount of either cold DOTA-MCG or DOTA-EB-MCG. The uptake and internalization rates at 24 h with blocking dropped significantly (Figure 1D). The internalization rate of ^{86}Y-DOTA-EB-MCG was also higher than that of ^{86}Y-DOTA-MCG (Figure 1B,C). Additionally, according to efflux assays, the washout rate for ^{86}Y-DOTA-EB-MCG after 4 h incubation was slower than ^{86}Y-DOTA-MCG (Figure 1D).

^{86}Y-Labeled PSMA Ligand PET Imaging.

The tumor uptake of ^{86}Y-DOTA-MCG and ^{86}Y-DOTA-EB-MCG was evaluated with both PC3 and PC3-PIP tumor models. ^{86}Y-DOTA-MCG showed remarkable tumor accumulation at early time points but much lower radioactivity was identified in the tumor region at later time points. The tracer cleared rapidly from the blood circulation, resulting in clear background in normal organs. ^{86}Y-DOTA-EB-MCG showed stronger tumor accumulation, especially at late stage.

Relatively high accumulation of ^{86}Y-DOTA-EB-MCG was observed in the kidneys. The tumor uptakes of ^{86}Y-DOTA-MCG and ^{86}Y-DOTA-EB-MCG in PC3 tumors were rather low due to the negligible PSMA expression level (Figure 2).

The uptakes of ^{86}Y-DOTA-MCG in PC-3 PIP tumors were 17.05 ± 3.66, 16.26 ± 4.09, 10.94 ± 1.70 and 4.80 ± 0.66%ID/ g at 1, 4, 24, and 48 h p.i., respectively. ^{86}Y-DOTA-EB-MCG showed much higher tumor uptake, which increased from 22.33 ± 2.39%ID/g at 1 h p.i. to the peak of 40.40 ± 4.79%ID/g at 24 h p.i. and remained high at 48 h p.i. (35.67 ± 4.27%ID/g) (Figure 3A). ^{86}Y-DOTA-EB-MCG also showed higher blood circulation and kidney retention compared with ^{86}Y-DOTA-MCG. The biodistribution studies of the two tracers in two tumor models confirmed the higher tumor uptake of ^{86}Y-DOTA-EB-MCG over ^{86}Y-DOTA-MCG (Figure S2). The uptake of ^{86}Y-DOTA-EB-MCG in PMSA negative PC3 tumors was 1.48 ± 0.25%ID/g at 48h p.i., as evaluated by biodistribution study (Figure S2).

To evaluate the radioactive dose delivery to the tumor and normal organs for ^{90}Y RLT, the time activity curves of tumor, kidneys, and blood, generated from ^{86}Y PET images, were replotted with the decay scheme of ^{90}Y and the results are presented in Figure 3B. The area under the curve (AUC) of ^{90}Y-DOTA-EB-MCG in PC-3 PIP tumors was 4.4 times higher than that of ^{90}Y-DOTA-MCG (1675.0 ± 89.9 vs 381.3 ± 43.31). AUCs of ^{90}Y-DOTA-EB-MCG over kidneys and blood were also much higher than those of ^{90}Y-DOTA-MCG (451.2 ± 35.16 vs 41.0 ± 6.9 and 194.1 ± 15.4 vs 6.4 ± 1.8, respectively; Figure 3B).

^{90}Y Radioligand Therapy.

Encouraged by the high cell internalization rate and tumor uptake value of ^{86}Y-DOTA-EB-MCG, we used EB-MCG in radioligand therapy after labeling it with ^{90}Y, a pure beta-emitting therapeutic radioisotope.

One-time injection of 7.4 MBq ^{90}Y-DOTA-MCG resulted in limited PC3-PIP tumor growth delay as compared with mice injected with saline. All the mice treated with saline or ^{90}Y-DOTA-MCG had to be sacrificed within 25 days due to the excessive tumor volume (Figure

4A). The tumors stopped growing for 20 days in the 3.7 MBq ^{90}Y-DOTA-EB-MCG treated group and started regrowing at around day 25 and mice were euthanized at around day 40. For mice treated with 7.4 MBq ^{90}Y-DOTA-EB-MCG, more significant tumor reduction was observed; however, tumor recurrence still occurred after day 40 (Figure 4B). No apparent body weight changes were found in mice injected with 3.7 MBq and 7.4 MBq ^{90}Y-DOTA-EB-MCG (Figure S3). No obvious differences were observed among the control and high-dose treatment groups as to the parameters acquired through blood analysis (Table S1). Minimum difference was noticed from the H&E staining results of noncancerous organs among different groups including saline control group and ^{90}Y treated groups (Figure S4).

With tumor sections from different treatment groups, immunofluorescence staining was performed to evaluate levels of PSMA and Ki67. TUNEL staining was also performed to detect DNA damage/cell apoptosis. The Ki67 signals for ^{90}Y-DOTA-EB-MCG treated groups were much less than those of saline and ^{90}Y-DOTA-MCG groups. Furthermore, tumors treated with higher radiation dose (7.4 MBq) showed much less Ki67 signal than those lower radiation dose (3.7 MBq) of ^{90}Y-DOTA-EB-MCG (Figure 5). The treatment also resulted in decreased PSMA level on the tumor sections. For the recurrent tumors, recovery of PSMA staining was identified, although the level of PSMA was lower than the saline treated tumors. The Ki67 level was also recovered to some extent (Figure 5).

DISCUSSION

As the most abundant protein in blood plasma (around 50 mg/ mL), albumin has been investigated as a drug carrier for decades, primarily for treating diabetes, cancer, rheumatoid arthritis, and infectious diseases.[27,28] It is well-known that the effectiveness of some pharmaceuticals is heavily dependent on their intrinsic pharmacokinetics, which can be improved by adding an albumin binding moiety.[29] Albumin-based drug delivery systems play a very important role in the treatment of diabetes and are also expanding to the field of oncology.[30,31] There are several unique advantages to introduce albumin-based delivery strategy into RLT. First of all, binding with albumin usually will extend the circulation time of the radioligands, resulting in increased interaction time frame of the radioligands to the receptors. Second, the relatively large size of the albumin–radioligand complex will facilitate tumor accumulation via the enhanced permeability and retention effect.[32] Moreover, additional internalization of the radioligand may be mediated by albumin-binding proteins such as gp60 receptor and SPARC (secreted protein acidic and rich in cysteine), which were found to be overexpressed in tumor environment.[33]

Although the detailed mechanism will need further investigation, increased tumor delivery and retention through the strategy of adding albumin binding moiety to radioligands have been proven in quite a few studies.[13,14,21,29,34] From example, using 4-(*p*-iodophenyl)butyric acid as an albumin binding moiety, the resulting folate conjugates showed significantly higher tumor uptake and retention over the unmodified folate.[34] Conjugation of the same albumin binding moiety with PSMA-617 led to almost doubled AUC within the tumor region compared to PSMA-617 alone.[14] Consequently, the tumor therapeutic efficacy was significantly improved with these “long-lasting” ligands after labeling with either ^{90}Y or ^{177}Lu. With truncated Evans blue as the albumin binding moiety,

^{90}Y-DOTA-EB-MCG also showed increased tumor delivery and retention with 4.4-fold increase of tumor AUC over ^{90}Y-DOTA-MCG. Therefore, the same dose of ^{90}Y-DOTA-EB-MCG exerted much better tumor therapeutic efficacy than ^{90}Y-DOTA-MCG. All these results demonstrated that RLT using albumin binding moieties modified small molecular ligands is a promising strategy in cancer management.

For RLT, kidneys are usually one of the critical organs in terms of radiation toxicity due to the fast clearance of radioligands through urinary tract and the presence of endogenous receptors within kidneys.[35–37] With 4-(*p*- iodophenyl)butyric acid conjugated folate, renal accumulation was somewhat reduced, compared with folate conjugates that lack an albumin-binding entity.[34] However, remarkably increased accumulation in the kidneys was observed with EB conjugated TATE than unconjugated TATE, a ligand that binds to somatostatin receptor subtype-2.[21] So far, both phosphoramidate-based and urea based PSMA ligands have been conjugated with 4-(*p*-iodophenyl)butyric acid for albumin binding.[13–15] After conjugation, all compounds showed much higher kidney accumulation than the unconjugated ligands. The kidney uptake of 4-(*p*-iodophenyl)butyric acid conjugated PSMA-617 was 11.4–34.9-fold higher than that of PSMA-617, depending on the different linkers used. In our study, AUC of ^{90}Y-DOTA-EB-MCG over kidneys was about 11-fold higher than that of ^{90}Y-DOTA-MCG (Figure 3B). The high kidney uptake may be related to extended circulation, endogenous expression of PSMA, and tubular reabsorption of albumin.Modification of the compound including usage of labile linkers and kidney specific degradable linkers is under investigation, with the aim of decreasing retention of EB-MCG in the kidneys.

The goal of RLT is to maximize the absorbed dose to the tumor while making the delivery to vulnerable normal organs within acceptable levels.[38] Significantly higher tumor uptake and accumulation was achieved by ^{90}Y-DOTA-EB-MCG over ^{90}Y-DOTA-MCG. Higher kidney accumulation was also identified. Moreover, the exposure to bone marrow was also increased due to the extended circulation time. However, no obvious systemic toxicity was observed by measuring body weight, blood chemistry, survival rate, and tissue histology with intravenous injection of 7.4 MBq ^{90}Y-DOTA-EB-MCG into PC3-PIP tumor mice. By balancing the benefit and risk, ^{90}Y-DOTA-EB-MCG at the therapeutic dose may have advantages over ^{90}Y-DOTA-MCG in prostate cancer treatment.

CONCLUSION

Modification of the urea-based PSMA ligand MCG with a truncated Evans blue moiety resulted in DOTA-EB-MCG, a highly efficient prostate cancer targeting agent that binds to both PSMA on the surface of cancer cell membrane and circulating albumin. DOTA-EB-MCG showed great potential in prostate cancer treatment after being labeled with therapeutic radioisotopes such as ^{90}Y.

MATERIALS AND METHODS

The synthesis and labeling of DOTA-MCG and DOTA-EB-MCG are described in the Supporting Information.

Cell Culture.

Human prostate cancer PC3 cell line was purchased from the American Type Culture Collection (ATCC, Manassas, VA). Both PSMA negative (PC3) and positive (PC3-PIP) cell lines were cultured in RPMI 1640 medium (Thermo Fisher Scientific) containing 10% Fetal Bovine Serum (FBS, GIBCO) in a humidified incubator containing 5% CO_2 at 37 °C.

Flow Cytometry.

All the solutions used in flow cytometry were kept at 4 °C before and during the test, PC3 and PC3-PIP cells were cultured in 75 cm^2 flasks and harvested at a density of 1×10^6 cells/mL in ice cold phosphate buffered saline (PBS) with 1% bovine serum albumin (BSA), cells were stained with 10 μL anti-PSMA or isotype antibody for 30 min at 4 °C in polystyrene round-bottom 12 × 75 mm tubes. Cells were washed with PBS three times and tested with an Accuri C6 plus cytometer (BD Biosciences, San Jose, CA).

Immunofluorescence Staining.

Different organs were harvested and imbedded in OCT and kept frozen at –80 °C. Frozen sections were cut into 10-μm-thick slices with cryostat. Different slices were fixed with z-fix for 30 min at room temperature and washed with PBS three times. 2% BSA in PBS was used to block the slices at room temperature for 1 h. Anti-PSMA antibody (Abcam ab133579, 1:150, 2% BSA in PBS) was added onto the slices and incubated at 4 °C overnight followed by PBS wash for 3 times (5 min each time). Goat-anti- rabbit secondary antibody (R&D, 1:100, 2% BSA in PBS) was added and slices were incubated for 1 h at room temperature. After washing with PBS three times, the slices were mounted with mounting solution containing DAPI. Fluorescence images were acquired by a fluorescence microscope (Olympus). Ki67, TUNEL, and H&E staining were also performed according to the kit instructions.

Cell Binding Assay.

Cell binding assay experiments were performed in triplicates using PSMA positive PC3-PIP cells. 10^5 PC3-PIP cells were added into membrane plate (Millipore) with 7.4 KBq of ^{86}Y-DOTA-MCG per well as well as gradient concentrations of unlabeled DOTA-MCG or DOTA-EB-MCG ranging 0–500 nM. After 1 h incubation, the plates were washed 3 times with PBS, then the membranes were heated to dry and counted with a gamma counter. The data were analyzed, and binding affinity was calculated with GraphPad Prism by nonlinear regression.

Cell Uptake/Internalization/Efflux Assays.

PC3-PIP cells were harvested and seeded in 24-well plates with 10^5 cells per well at 24 h before the assay. After removing the medium and washing the cells once with PBS, 7.4 KBq of ^{86}Y- DOTA-MCG or ^{86}Y-DOTA-EB-MCG in 500 μL was added into each well in RPMI 1640 medium containing 1% (w/v) human serum albumin. The cells were incubated at 37 °C for 1, 4, and 24 h. At each indicated time point, the medium was aspirated and cells were washed with 1 mL PBS twice. Then, 0.2 mL 0.1 M NaOH (lysis buffer) was added to each well to collect the cells for gamma counting.

For cell internalization assay, each experiment was repeated twice in triplicate. After the removal of cell medium at each indicated time point, the cells were incubated with 0.5 mL acid wash buffer (50 mM Glycine, 100 mM NaCl, pH 2.8) for 1 min. Then the acid wash buffer was removed, and the cells were washed twice with PBS, followed by adding 0.2 mL 0.1 M NaOH. Cell lysate was collected, and radioactivity was measured with a gamma counter. Cell uptake and internalization values were normalized with the total amount of added radioactivity.

For cell efflux assay, 7.4 KBq of ^{86}Y-DOTA-MCG or ^{86}Y-DOTA-EB-MCG was added to PC3-PIP cells in a 24-well plate and incubated for 4 h at 37 °C. The cells were washed twice with cold PBS and incubated with radioactivity free medium for 1, 4, and 24 h. After washing twice with cold PBS, cells were harvested by adding 0.2 mL 0.1 M NaOH for gamma counting.

Mouse Xenograft Models.

All tumor models were prepared under a protocol approved by the NIH Clinical Center Animal Care and Use Committee (ACUC). Seven- to eight-week-old male mice (Athymic Nude-Foxn1nu, Envigo) were inoculated with 5×10^6 cells (PC3 or PC3-PIP with Matrigel 1:1, total volume 100 μL) onto the right shoulder. Tumor volume was monitored by caliper measurement.

In Vivo PET Imaging and Biodistribution Study.

PET imaging studies were performed 2–3 weeks after tumor inoculation when the tumor size reached around 300 mm^3. ^{86}Y-DOTA-MCG or ^{86}Y-DOTA-EB-MCG (3.7–5.1 MBq in 100 μL buffer) was injected intravenously to each tumor mouse (n = 6/group) and the mice were scanned for 10–20 min at 1, 4, 24, and 48 h post-injection (p.i.). PET images were acquired on an Inveon small animal PET scanner (Siemens Preclinical Solutions, Knoxville, TN) and reconstructed by ASIPRO software provided by the manufacturer. Biodistribution study was carried out after PET scan at 48 h time point. Tumor and normal organs were collected, weighed, and measured with a gamma counter. Results were normalized as percentages of the injected dose per gram of organ (%ID/g).

Radioligand Therapy.

Tumor radiotherapy studies started when the tumor reached volume about 150 mm^3 (about 7 days after inoculation of PC3-PIP cells and 10 days after inoculation of PC3 cells). Mice were randomly divided into 4 groups (5–6 mice per group) to receive single injection of saline, 7.4 MBq ^{90}Y-DOTA-MCG, 3.7 MBq ^{90}Y-EB-MCG, or 7.4 MBq ^{90}Y-EB- MCG. Tumor volume, body weight, and survival rate were monitored. Tumor volume was calculated by width^2 × length/ 2. All the live mice were monitored for 42 days. End point for each animal was defined by the ACUC protocol as 15% body weight loss or tumor volume over 1800 mm^3.

Statistical Analysis.

All the data were analyzed with GraphPad Prism or Microsoft Excel. Results were shown with mean ± SD. The differences within groups and between groups were determined with two-tailed paired and unpaired Student's *t* tests, respectively.

Supplementary Material

Refer to Web version on PubMed Central for supplementary material.

ACKNOWLEDGMENTS

This work was supported by the Intramural Research Program of the National Institute of Biomedical Imaging and Bioengineering (NIBIB), National Institutes of Health (NIH) as well as NIH grants CA134675 and CA184228 (M.G. Pomper).

REFERENCES

(1). Torre LA, Bray F, Siegel RL, Ferlay J, Lortet-Tieulent J, and Jemal A (2015) Global Cancer Statistics, 2012. Ca-Cancer J. Clin. 65 (2), 87–108. [PubMed: 25651787]

(2). Weiner AB, and Kundu SD (2018) Prostate Cancer: A Contemporary Approach to Treatment and Outcomes. Med. Clin. North Am. 102 (2), 215–229. [PubMed: 29406054]

(3). Fendler WP, Rahbar K, Herrmann K, Kratochwil C, and Eiber M (2017) ^{177}Lu-PSMA Radioligand Therapy for Prostate Cancer. J. Nucl. Med. 58 (8), 1196–1200. [PubMed: 28663195]

(4). Maurer T, Eiber M, Schwaiger M, and Gschwend JE (2016) Current Use of PSMA-PET in Prostate Cancer Management. Nat. Rev. Urol. 13 (4), 226–235. [PubMed: 26902337]

(5). Eiber M, Fendler WP, Rowe SP, Calais J, Hofman MS, Maurer T, Schwarzenboeck SM, Kratowchil C, Herrmann K, and Giesel FL (2017) Prostate-Specific Membrane Antigen Ligands for Imaging and Therapy. J. Nucl. Med. 58 (Suppl 2), 67S–76S. [PubMed: 28864615]

(6). Machulkin AE, Ivanenkov YA, Aladinskaya AV, Veselov MS, Aladinskiy VA, Beloglazkina EK, Koteliansky VE, Shakhbazyan AG, Sandulenko YB, and Majouga AG (2016) Small-Molecule PSMA Ligands. Current State, Sar and Perspectives. J. Drug Target 24 (8), 679–693. [PubMed: 26887438]

(7). Bouchelouche K, Turkbey B, and Choyke PL (2016) PSMA PET and Radionuclide Therapy in Prostate Cancer. Semin. Nucl. Med. 46 (6), 522–535. [PubMed: 27825432]

(8). Kopka K, Benesova M, Barinka C, Haberkorn U, and Babich J (2017) Glu-Ureido-Based Inhibitors of Prostate-Specific Membrane Antigen: Lessons Learned During the Development of a Novel Class of Low-Molecular-Weight Theranostic Radiotracers. J. Nucl. Med. 58 (Suppl 2), 17S–26S. [PubMed: 28864607]

(9). Baum RP, Kulkarni HR, Schuchardt C, Singh A, Wirtz M, Wiessalla S, Schottelius M, Mueller D, Klette I, and Wester HJ (2016) ^{177}Lu-Labeled Prostate-Specific Membrane Antigen Radioligand Therapy of Metastatic Castration-Resistant Prostate Cancer: Safety and Efficacy. J. Nucl. Med. 57 (7), 1006–1013. [PubMed: 26795286]

(10). Yadav MP, Ballal S, Tripathi M, Damle NA, Sahoo RK, Seth A, and Bal C (2017) ^{177}Lu-Dkfz-PSMA-617 Therapy in Metastatic Castration Resistant Prostate Cancer: Safety, Efficacy, and Quality of Life Assessment. Eur. J. Nucl. Med. Mol. Imaging 44 (1), 81–91.

(11). Rahbar K, Bode A, Weckesser M, Avramovic N, Claesener M, Stegger L, and Bogemann M (2016) Radioligand Therapy with ^{177}Lu-PSMA-617 as a Novel Therapeutic Option in Patients with Metastatic Castration Resistant Prostate Cancer. Clin Nucl. Med. 41 (7), 522–528. [PubMed: 27088387]

(12). Weineisen M, Schottelius M, Simecek J, Baum RP, Yildiz A, Beykan S, Kulkarni HR, Lassmann M, Klette I, Eiber M, Schwaiger M, and Wester HJ (2015) ^{68}Ga- and ^{177}Lu-Labeled PSMA I&T: Optimization of a PSMA-Targeted Theranostic Concept and First Proof-of-Concept Human Studies. J. Nucl. Med. 56 (8), 1169–1176. [PubMed: 26089548]

(13). Choy CJ, Ling X, Geruntho JJ, Beyer SK, Latoche JD, Langton-Webster B, Anderson CJ, and Berkman CE (2017) ^{177}Lu-Labeled Phosphoramidate-Based PSMA Inhibitors: The Effect of an Albumin Binder on Biodistribution and Therapeutic Efficacy in Prostate Tumor-Bearing Mice. Theranostics 7 (7), 1928–1939. [PubMed: 28638478]

(14). Benesova M, Umbricht CA, Schibli R, and Muller C (2018) Albumin-Binding PSMA Ligands: Optimization of the Tissue Distribution Profile. Mol. Pharmaceutics 15 (3), 934–946.

(15). Kelly J, Amor-Coarasa A, Ponnala S, Nikolopoulou A, Williams C, Jr., Schlyer D, Zhao Y, Kim D, and Babich JW (2018) Trifunctional PSMA-Targeting Constructs for Prostate Cancer with Unprecedented Localization to Lncap Tumors. Eur. J. Nucl. Med. Mol. Imaging, 1–11.

(16). Niu G, Lang L, Kiesewetter DO, Ma Y, Sun Z, Guo N, Guo J, Wu C, and Chen X (2014) In Vivo Labeling of Serum Albumin for PET. J. Nucl. Med. 55 (7), 1150–1156. [PubMed: 24842890]

(17). Wang Y, Lang L, Huang P, Wang Z, Jacobson O, Kiesewetter DO, Ali IU, Teng G, Niu G, and Chen X (2015) In Vivo Albumin Labeling and Lymphatic Imaging. Proc. Natl. Acad. Sci. U. S. A. 112 (1), 208–213. [PubMed: 25535368]

(18). Zhang J, Lang L, Zhu Z, Li F, Niu G, and Chen X (2015) Clinical Translation of an Albumin-Binding PET Radiotracer ^{68}Ga- NEB. J. Nucl. Med. 56 (10), 1609–1614. [PubMed: 26251416]

(19). Long X, Zhang J, Zhang D, Gao C, Chi C, Yang E, Xue H, Lang L, Niu G, Zhu Z, Li F, and Chen X (2017) Microsurgery Guided by Sequential Preoperative Lymphography Using ^{68}Ga-NEB PET and Mri in Patients with Lower-Limb Lymphedema. Eur. J. Nucl. Med. Mol. Imaging 44 (9), 1501–1510.

(20). Chen H, Tong X, Lang L, Jacobson O, Yung BC, Yang X, Bai R, Kiesewetter DO, Ma Y, Wu H, Niu G, and Chen X (2017) Quantification of Tumor Vascular Permeability and Blood Volume by Positron Emission Tomography. Theranostics 7 (9), 2363–2376. [PubMed: 28744320]

(21). Tian R, Jacobson O, Niu G, Kiesewetter DO, Wang Z, Zhu G, Ma Y, Liu G, and Chen X (2018) Evans Blue Attachment Enhances Somatostatin Receptor Subtype-2 Imaging and Radiotherapy. Theranostics 8 (3), 735–745. [PubMed: 29344302]

(22). Zhang J, Wang H, Jacobson Weiss O., Cheng Y, Niu G, Li F, Bai C, Zhu Z, and Chen X (2018) Safety, Pharmacokinetics and Dosimetry of a Long-Acting Radiolabeled Somatostatin Analogue ^{177}Lu-Dota-Eb-Tate in Patients with Advanced Metastatic Neuroendocrine Tumors. J. Nucl. Med, DOI: 10.2967/jnumed.118.209841.

(23). Kozikowski AP, Nan F, Conti P, Zhang J, Ramadan E, Bzdega T, Wroblewska B, Neale JH, Pshenichkin S, and Wroblewski JT (2001) Design of Remarkably Simple, yet Potent Urea-Based Inhibitors of Glutamate Carboxypeptidase II (Naaladase). J. Med. Chem. 44 (3), 298–301. [PubMed: 11462970]

(24). Pomper MG, Musachio JL, Zhang J, Scheffel U, Zhou Y, Hilton J, Maini A, Dannals RF, Wong DF, and Kozikowski AP (2002) ^{11}C-MCG: Synthesis, Uptake Selectivity, and Primate PET of a Probe for Glutamate Carboxypeptidase Ii (Naaladase). Mol. Imaging 1 (2), 96–101. [PubMed: 12920850]

(25). Foss CA, Mease RC, Fan H, Wang Y, Ravert HT, Dannals RF, Olszewski RT, Heston WD, Kozikowski AP, and Pomper MG (2005) Radiolabeled Small-Molecule Ligands for Prostate-Specific Membrane Antigen: In Vivo Imaging in Experimental Models of Prostate Cancer. Clin. Cancer Res. 11 (11), 4022–4028. [PubMed: 15930336]

(26). Mease RC, Dusich CL, Foss CA, Ravert HT, Dannals RF, Seidel J, Prideaux A, Fox JJ, Sgouros G, Kozikowski AP, and Pomper MG (2008) N-[N-[(S)-1,3-Dicarboxypropyl]- Carbamoyl]-4-[^{18}F]Fluorobenzyl-L-Cysteine, [^{18}F]DCFBC: A New Imaging Probe for Prostate Cancer. Clin. Cancer Res. 14 (10), 3036–3043. [PubMed: 18483369]

(27). Elsadek B, and Kratz F (2012) Impact of Albumin on Drug Delivery-New Applications on the Horizon. J. Controlled Release 157 (1), 4–28.

(28). Liu Z, and Chen X (2016) Simple Bioconjugate Chemistry Serves Great Clinical Advances: Albumin as a Versatile Platform for Diagnosis and Precision Therapy. Chem. Soc. Rev. 45 (5), 1432–1456. [PubMed: 26771036]

(29). Chen H, Jacobson O, Niu G, Weiss ID, Kiesewetter DO, Liu Y, Ma Y, Wu H, and Chen X (2017) Novel “Add-on” Molecule Based on Evans Blue Confers Superior Pharmacokinetics and Transforms Drugs to Theranostic Agents. J. Nucl. Med. 58 (4), 590–597. [PubMed: 27879373]

(30). Larsen MT, Kuhlmann M, Hvam ML, and Howard KA (2016) Albumin-Based Drug Delivery: Harnessing Nature to Cure Disease. Mol. Cell Ther 4, 3. [PubMed: 26925240]

(31). Thrasher J (2017) Pharmacologic Management of Type 2 Diabetes Mellitus: Available Therapies. Am. J. Cardiol. 120 (1S), S4–S16. [PubMed: 28606343]

(32). Maeda H, Wu J, Sawa T, Matsumura Y, and Hori K (2000) Tumor Vascular Permeability and the Epr Effect in Macromolecular Therapeutics: A Review. J. Controlled Release 65 (1–2), 271–284.

(33). Merlot AM, Kalinowski DS, and Richardson DR (2014) Unraveling the Mysteries of Serum Albumin-More Than Just a Serum Protein. Front. Physiol. 5, 299. [PubMed: 25161624]

(34). Muller C, Struthers H, Winiger C, Zhernosekov K, and Schibli R (2013) Dota Conjugate with an Albumin-Binding Entity Enables the First Folic Acid-Targeted ^{177}Lu-Radionuclide Tumor Therapy in Mice. J. Nucl. Med. 54 (1), 124–131. [PubMed: 23236020]

(35). Del Prete M, Buteau FA, and Beauregard JM (2017) Personalized ^{177}Lu-Octreotate Peptide Receptor Radionuclide Therapy of Neuroendocrine Tumours: A Simulation Study. Eur. J. Nucl. Med. Mol. Imaging 44, 1490.

(36). Kwekkeboom DJ, de Herder WW, Kam BL, van Eijck CH, van Essen M, Kooij PP, Feelders RA, van Aken MO, and Krenning EP (2008) Treatment with the Radiolabeled Somatostatin Analog [^{177}Lu-DOTA^{0},Tyr^{3}]Octreotate: Toxicity, Efficacy, and Survival. J. Clin. Oncol. 26 (13), 2124–2130. [PubMed: 18445841]

(37). Cives M, and Strosberg J (2017) Radionuclide Therapy for Neuroendocrine Tumors. Curr. Oncol. Rep. 19 (2), 9.

(38). Schwartz J, Humm JL, Divgi CR, Larson SM, and O'Donoghue JA (2012) Bone Marrow Dosimetry Using ^{124}I-PET. J. Nucl. Med. 53 (4), 615–621. [PubMed: 22414633]

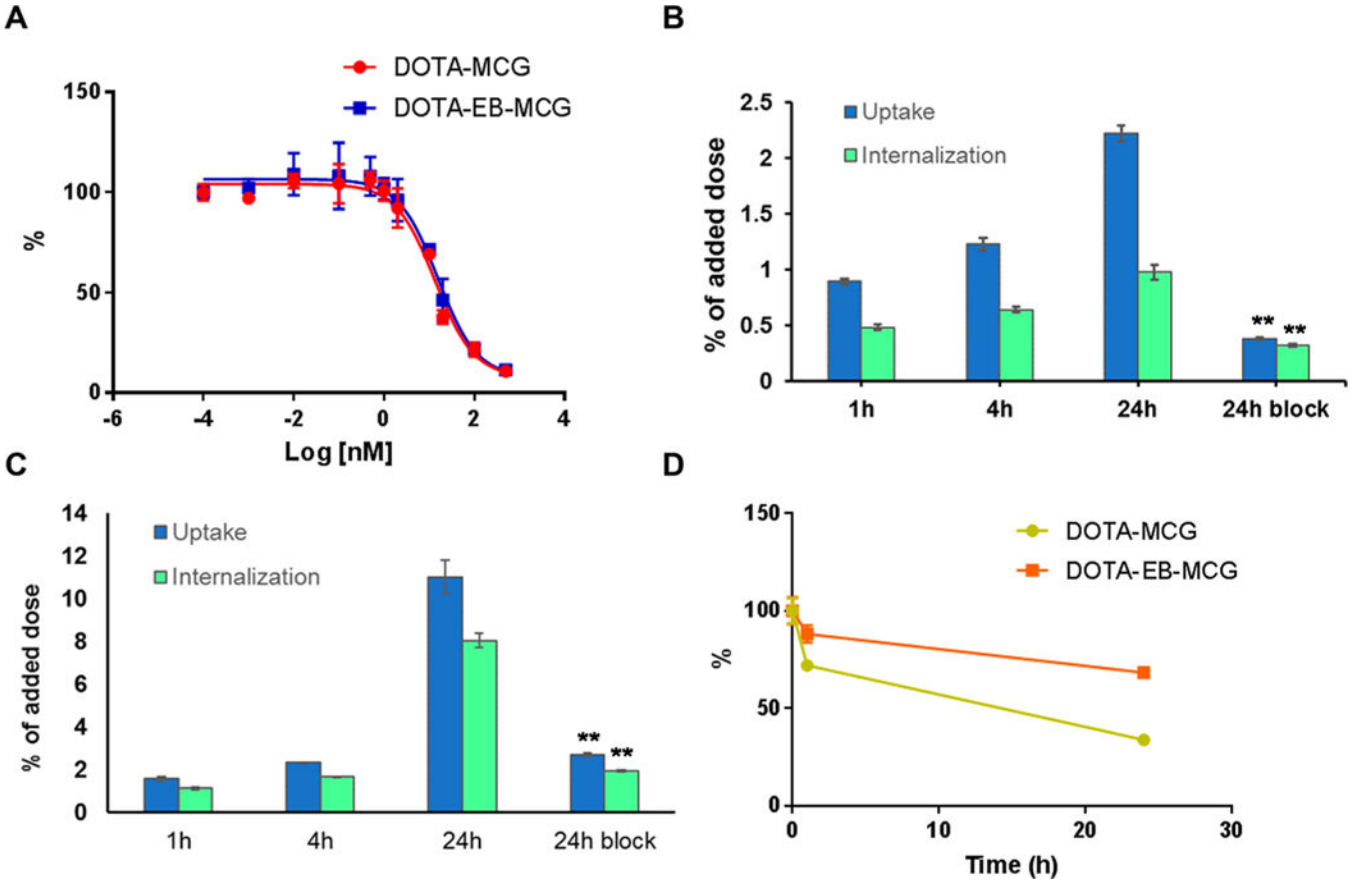

Figure 1.

(A) Cell binding assays of DOTA-EB-MCG and DOTA-MCG in PC3-PIP cells. (B) Cell uptake and internalization assay of ^{86}Y-DOTA- MCG in PC3-PIP cells. (C) Cell uptake and internalization assay of ^{86}Y- DOTA-EB-MCG in PC3-PIP cells. (D) Cell efflux assays of ^{86}Y-DOTA- MCG and ^{86}Y-DOTA-EB-MCG.

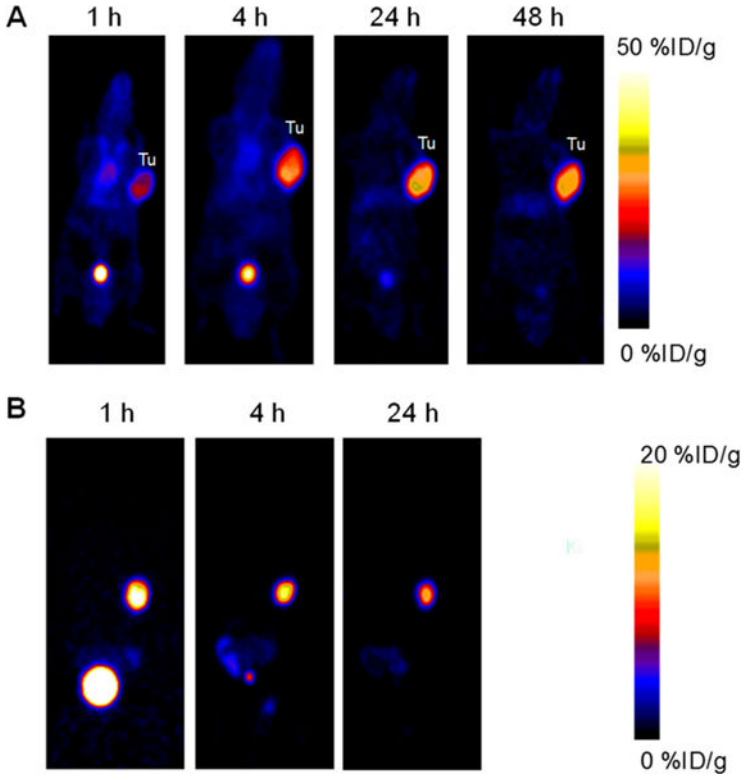

Figure 2.

Coronal PET images of PC3-PIP tumor mice at different time points after intravenous injection of ^{86}Y-DOTA-EB-MCG (A) and 86Y-DOTA-MCG (B). The PET image of ^{86}Y-DOTA-MCG at 48 h time point was not presentable due to the almost complete clearance of the tracer and extremely low counts.

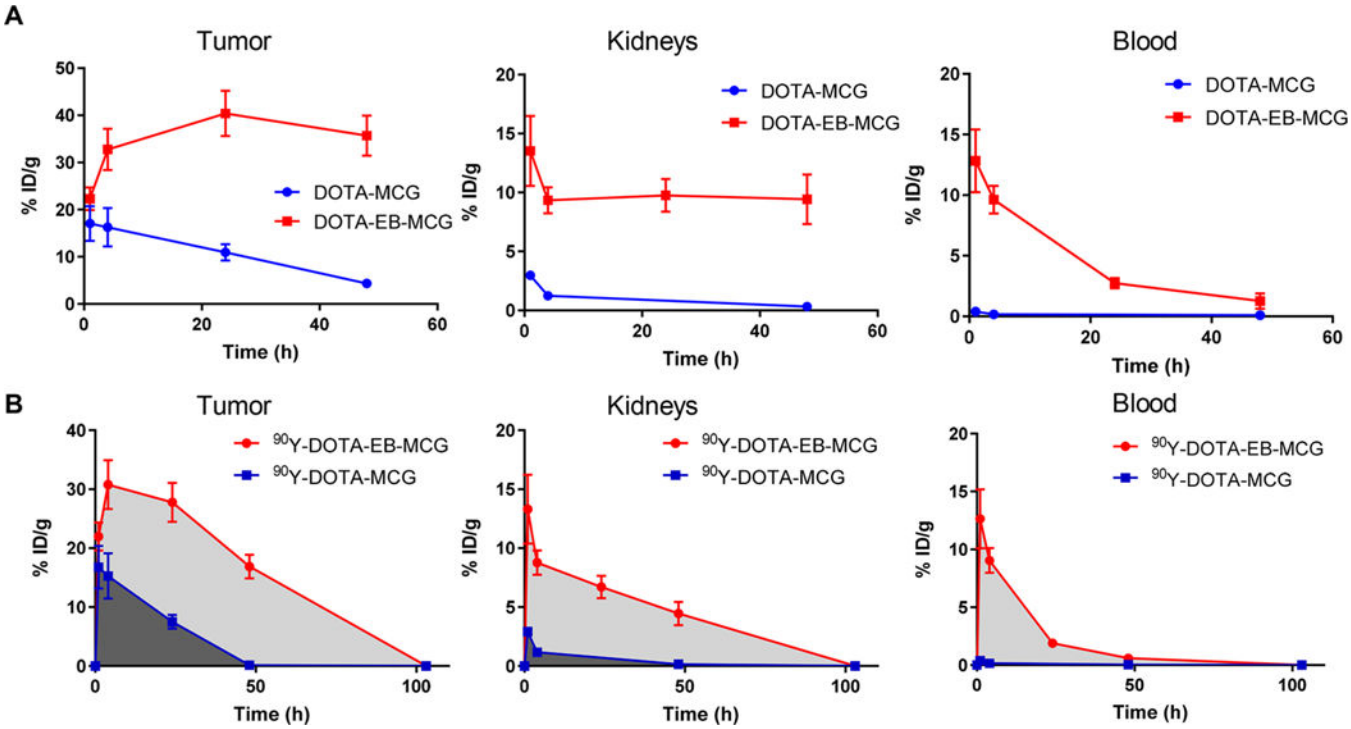

Figure 3.

(A) Time activity curves of ^{86}Y-DOTA-EB-MCG and ^{86}Y- DOTA-EB-MCG in the PC3-PIP tumor, kidneys and blood. (B) Comparison of area under the curve (AUC) between ^{90}Y-DOTA-EB-MCG and ^{90}Y-DOTA- MCG over tumor, kidneys, and blood. The curves were plotted with the decay scheme of ^{90}Y for calculating residence time.

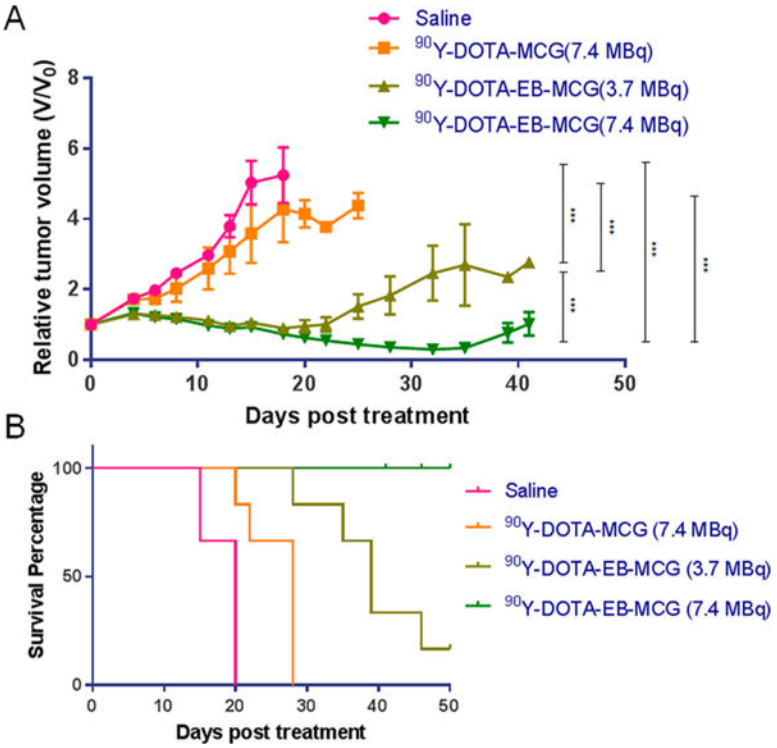

Figure 4.

Radionuclide tumor therapy with ^{90}Y. A. Tumor growth curve of mice bearing PC3-PIP tumor after injection of saline, 7.4 MBq ^{90}Y-DOTA-MCG, 3.7 MBq ^{90}Y-DOTA-EB-MCG, and 7.4 MBq ^{90}Y-DOTA-EB-MCG. B. Mouse survival curve in the four groups. (***, $P <$ 0.0001).

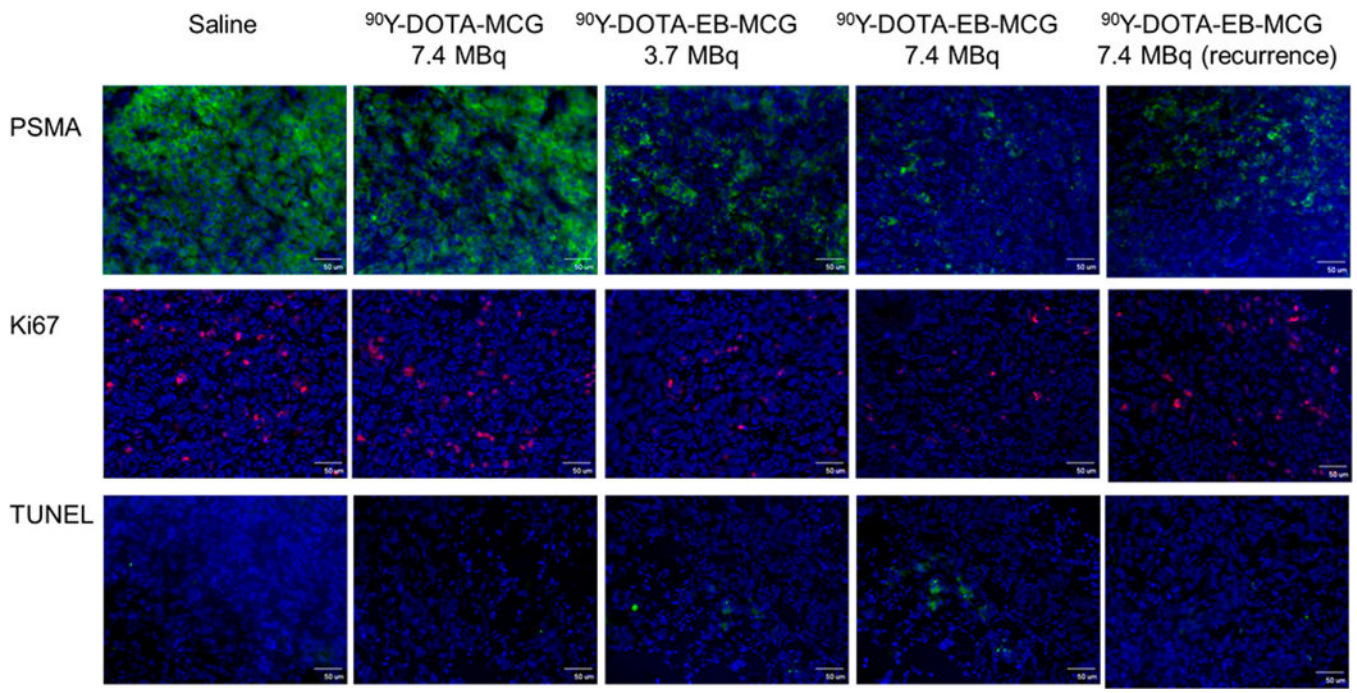

Figure 5.

Tumor biology evaluation after ^{90}Y radioligand therapy. Frozen section immunofluorescence staining on excised PC3-PIP tumors for PSMA expression levels (green), Ki67 (red) and TUNEL (green) with nuclei stained with DAPI (blue). Scale bar: 50 μm.